 CMC, vol.14, no.3, pp.185-196, 2009

EBSD-Based Microscopy: Resolution of Dislocation Density

Brent L. Adams and Joshua Kacher

Abstract: Consideration is given to the resolution of dislocation density afforded by EBSD-based scanning electron microscopy. Comparison between the conventional Hough- and the emerging high-resolution cross-correlation-based approaches is made. It is illustrated that considerable care must be exercised in selecting a step size (Burger's circuit size) for experimental measurements. Important variables affecting this selection include the dislocation density and the physical size and density of dislocation dipole and multi-pole components of the structure. It is also illustrated that simulations can be useful to the interpretation of experimental recoveries.

Keywords: electron diffraction, EBSD, dislocation density tensor

1 Introduction

Electron backscatter diffraction (EBSD)-based microscopy is now standard practice in many materials laboratories worldwide. A recent monograph, entitled *Electron Backscatter Diffraction in Materials Science*, reviews state-of-the-art practice in EBSD-based electron microscopy, including many applications (Schwartz 2000). The purpose of this paper is to consider future applications of the emerging High-Resolution EBSD microscopy (hereafter HR-EBSD), particularly in relation to structural materials where defect-sensitive mechanical properties, related to the state of dislocation, are of paramount importance.

Approximately twelve years ago (1997) the author reviewed emerging and future applications of conventional EBSD-microscopy (Adams 1997). Typical spatial and angular resolutions at that time were reported to be $\sim$100nm and 1^0, respectively. Temporal resolution, associated with the rate at which EBSD patterns could be collected and analyzed, was approximately 2 points per second. Significant improvements in resolution have been achieved in modern EBSD systems. Current resolution limits for EBSD-based microscopy are approximately 20nm spatial, 0.006^0 angular; and data acquisition rates approach 10^3 s^{-1}, although these resolution

limits are not presently achieved simultaneously. These changes in resolution profoundly influence the nature of EBSD-based microscopy, and the microstructure-based properties that can now be investigated.

The premise of this paper is that HR-EBSD-based microscopy is well positioned to elucidate some of the most important and challenging contemporary materials problems – problems that relate to the polarization of stress in heterogeneous materials. However, great care must be exercised in the measurement and interpretation of fundamental measurements of dislocation density. Selection of step size, considerations of instrument resolution and noise, and the interpretation of recovered dislocation density information are the principal topics of this paper.

2 HR-EBSD Measurements, Orientation and Strain Analysis

Accurate measurements of the field of dislocation in ductile polycrystalline materials can provide valuable information for the study of defect-sensitive phenomena, such as the mechanisms of plastic deformation, formability, electrical resistance, and likely failure sites under conditions of fatigue and creep. The measurement and characterization of dislocation fields remains a challenging problem. HR-EBSD is a valuable tool for the characterization of continuum dislocation structure. Relatively large areas of a sample can be analyzed in reasonable experimental times to provide information on the local crystallographic orientation and, using more recent cross-correlation methods, lattice curvature and elastic strain. Here we critically examine the capabilities of EBSD methods for dislocation density estimations with a focus on resolution and step size considerations when using such methods. For comparison, two EBSD methods are presented in this work, traditional Hough-based orientation analysis and the more recent cross-correlation method introduced by Troost and refined by Wilkinson (Troost, Van der Sluis et al. 1993; Wilkinson, Meaden et al. 2005).

In the traditional Hough-based method, the Kikuchi bands in the EBSD pattern are converted into peaks in Hough space. With the Hough (Radon) transform, lines become points and bands become spots. Intensity maxima are identified in the spot pattern, and their positions are used to index the EBSD pattern for lattice orientation, using crystallographic data for known phases. Indexing speeds in excess of 800 points/s have been reported. The angular resolution of the Hough-based method is commonly reported to be $\sim$0.5 degrees (Wright 1993).

The cross-correlation method relies on direct comparisons of EBSD patterns at a number of corresponding 'regions of interest' (ROI) within the patterns. The shift that best aligns the features in corresponding ROIs is measured using the cross-correlation function. These shifts in the patterns can be related to elastic deforma-

tion of the crystal lattice according to the following formula:

$$\vec{q} = \vec{w} - (\vec{w} \cdot \hat{r})\hat{r} \tag{1}$$

where

$$\vec{w} = U\hat{r} \tag{2}$$

$\vec{q}$ is the shift measured on the phosphor screen using the cross-correlation function, $\hat{r}$ is a unit vector pointing from the sample to the center of the ROI on the phosphor, and U is the displacement gradient tensor. By rewriting equation (1) in component form, the $w \cdot \hat{r}$ term can be eliminated to reduce the system to two equations. If the shifts in the EBSD pattern are measured at four or more regions, eight of the nine components of U can be recovered. The ninth component is the spherical strain, which causes no shift in the position of features within the EBSD patterns, but an expansion or contraction of the size of those features which is not easily resolved. This unresolved spherical strain can be determined if a traction-free boundary condition is added to the system of equations (1, 2). Applying this added condition requires knowledge of the local elastic constants at the material point to be examined. For polycrystalline materials this is available if the basic elastic constants of the constituent phase is known, when coupled with the local lattice orientation, through the standard transformation laws for fourth rank tensors. U can be further decomposed into symmetric and asymmetric parts corresponding to the infinitesimal elastic strain gradient and rotation tensors respectively. The cross-correlation method is capable of measuring misorientations to within $+/-0.006^{\circ}$ and components of the elastic strain tensor to within $+/-1.6\times10^{-4}$ (Wilkinson, Meaden et al. 2006). The cross-correlation method and resolution limits, originally reported by Wilkinson, have been reproduced by the authors (Kacher, Landon et al. 2009).

3 Determination of Continuum Dislocation Densities

The theoretical groundwork for dislocation density estimates is largely based on the work of Nye (Nye 1953). He was able to show how the lattice curvature, or curl of the orientation field, could be linked to geometrically necessary dislocations (GNDs). Later work by Kröner advanced Nye's work to include the elastic strain gradient in the formulation (Kroner 1958). The following equation emerged (Sun, Adams et al. 2000):

$$\alpha_{ik} = \kappa_{ki} - \delta_{ki}\kappa_{pp} + e_{klj}\varepsilon^{e}_{ij,l} \tag{3}$$

where κ_{ki} is the lattice curvature and is given by:

$$\kappa_{ki} = \frac{\partial \theta_k}{\partial x_i} \tag{4}$$

$\varepsilon^e_{ij,l}$ is the *jth* spatial derivative of the elastic strain, e_{klj} is the Levi Cevita symbol, δ_{ki} is the Kronecker delta function, and α_{ik} is the dislocation density tensor. The components of the dislocation density tensor weight the dyadic formed by the direction of the dislocation line and the Burgers' vector characterizing that dislocation. When the data obtained is limited to a two-dimensional plane, the dislocation density tensor can only be partially resolved. Any out of plane derivatives, or derivatives with respect to x_3, are unobtainable. This limits the measurable components of the dislocation density tensor to α_{i3}. Additionally, α_{12} and α_{21} are also resolvable when contributions from the elastic strain are ignored (Pantleon 2008).

It is important to emphasize that the Nye formulation is dependent on measuring the net Burgers' vector within a single Burgers' circuit. When estimating dislocation densities using EBSD, a Burgers' circuit is formed by a square grid of four EBSD measurement points. The orientation and elastic strain information can be collected at each corner of the circuit and used to estimate the dislocation density within the circuit (Pantleon 2008). Statistically stored dislocations (SSDs) occur in dipoles and multipoles with no net Burgers' vector when their poles fall within the prescribed Burger's circuit. SSDs can be detected only when the size of the Burgers' circuit is small enough to separate the poles for individual detection (Kacher, Landon et al. 2009).

When estimating dislocation densities using EBSD, it is vital that an appropriate step size is used. It has been estimated that the critical distance at which dislocations will self annihilate is ∼20 atomic distances (Kroner 1958). Ideally, there would be a method with sufficient spatial and angular resolution that each dislocation could be individually resolved. However, both spatial and angular limitations of current EBSD-based techniques make this infeasible. There are two competing considerations when choosing a step size. Nye's formulation for dislocation density is dependent on spatial derivatives. It follows that as the step size decreases, any measurement error of the data is amplified. While increasing the step size does reduce the effect of noise in the data, it has an adverse effect in that important information on dislocation networks can be lost. As stated previously, any dislocations with opposing signs within a single Burgers' circuit have no effect upon the net Burgers' vector detected within the circuit, and so remain undetected.

The limiting dislocation density resolution of any EBSD method can be expressed as a function of the angular resolution of the applied method (conventional Hough-based method or the high resolution cross-correlation method) and the chosen step size.

$$\rho^{GND}_{\min} = \frac{\theta_{\min}}{Lb} \tag{5}$$

where $\theta_{\min}$ is the limiting angular resolution of the chosen method in radians, L

is the step size, and b is the magnitude of the Burgers' vector. When equation (5) is plotted for these two methods, it can act as a guide for both the selection of an appropriate step size and the interpretation of dislocation density data obtained. Assuming a Burgers' vector of 2.5 Å, the minimum resolvable dislocation density is plotted as a function of step size for both the traditional Hough-based method and the cross-correlation method (Figure 1). The interpretation of the plot is that any dislocation density that falls below the minimum resolvable dislocation density line will be dominated by noise, and is thus unobtainable by the selected technique. Any measured dislocation density that falls along the line corresponding to the selected technique should not be treated as an accurate estimate since it is not possible to determine whether the effect is from noise or if the physical dislocation density is being measured.

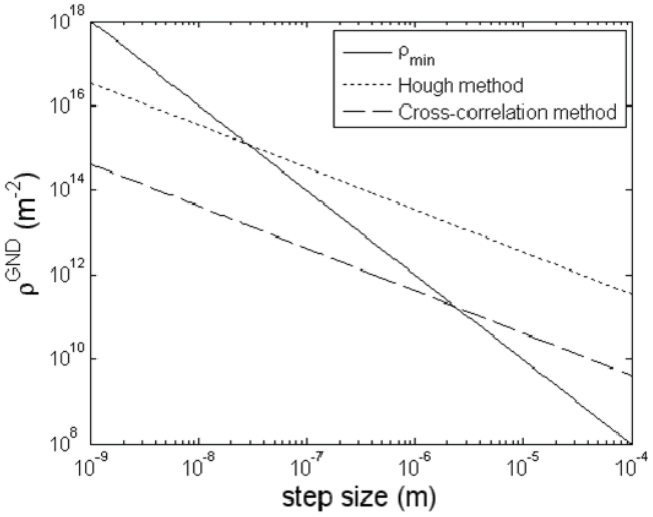

Figure 1: Dislocation density resolution estimates

Another line (solid line in Figure 1) is plotted showing the physically feasible dislocation density measureable as a function of step size. Any data falling below this line corresponds to a non-physical fraction of a dislocation per Burgers' circuit. This minimum dislocation density is given by:

$$\rho_{\min} = \frac{1}{L^2} \tag{6}$$

$\rho_{\min}$ is the dislocation density corresponding to one dislocation per Burgers' circuit. It should be emphasized that this analysis refers to the local dislocation density (at

the level of one Burgers' circuit). It is often the case that the dislocation density will vary significantly over a single grain such as when dislocations pile up near grain boundaries. These local variations in dislocation density should be taken into account when choosing a step size. Future schemes to address this issue dynamically could include adaptive alterations of the step size according to the current dislocation density recoveries.

Average dislocation densities have been commonly measured to be $\sim 10^{13}$-10^{16} m^{-2}. As can be seen in Figure 1, because of angular resolution limitations in the Hough-based method, a relatively large step size must be used to resolve such dislocation densities. However, this increases the risk that many of the dislocations will be averaged out within the Burgers' circuit, thereby reducing the estimated dislocation density. By increasing the angular resolution using the cross-correlation method, the resolution of dislocation density estimates can be improved by almost two orders of magnitude over traditional Hough-based techniques. This improvement in resolution of the local state of dislocation will be particularly important to studies of elastic/plastic polarization and their effects on defect nucleation.

4 Simulations of EBSD Resolution

To demonstrate the effect of angular resolution on dislocation density estimates, a number of dislocation networks in a material was simulated. The simulation is a simplified model where only one type of edge dislocation is considered. The dislocation line direction is fixed perpendicular to the Burger's circuit. Two possible Burgers' vectors were allowed, pointing in either the positive or negative directions, perpendicular to the fixed dislocation line direction. Two-dimensional networks were simulated to have a random spatial placement of dislocations, and a random assignment of Burger's vector. Total dislocation densities were prescribed. Also, under the conditions set for the simulations, a small bias between the two types of Burger's vectors was allowed, resulting in roughly 4% of the dislocations being geometrically necessary for each of the simulations. The total area simulated was a 10×10 μm square. At this size, the total dislocation content for $\rho^{tot} = 10^{16}m^{-2}$ is 10^6, for $\rho^{tot} = 10^{15}m^{-2}$ the total dislocation content is 10^5, and so on. Using these simulated networks, the dislocation density was estimated at increasing step sizes using square Burger's circuits. Mean values of multiple samplings of the complete simulated field are reported as dislocation densities at a specified step size. A noise component was added to the measured data that corresponds to the angular resolution of each technique. The magnitude of the added noise varied randomly between zero and the value given by Equation 5. The recovered (mean) dislocation densities, as a function of step size, are shown for each of the two methods in Figure 2. For comparison, reference points were also plotted with no noise component. The

lines from Figure 1, indicating the estimated resolution limits, are also plotted in Figure 2.

The following observations can be drawn from the simulated data. First, it can be seen that the data follows a general trend of reaching an upper plateau (left side) at the total dislocation density. This occurs whenever the resolution limit of the method lies below the simulation density. For example, at $10^{13}\mathrm{m}^{-2}$ the cross-correlation method plateaus at a step size of $\sim 10^{-7}$m but rejoins the line indicating its resolution limit at about $8\mathrm{x}10^{-7}$m, where the results are dominated by noise. At the same simulated density it is obvious that no useful information can be obtained from the conventional Hough-based method, which is dominated by noise over the entire range of step sizes. This plateau, for every case except for highest simulated dislocation density, $10^{16}\mathrm{m}^{-2}$, is reached at a significantly larger step size than the minimum plotted step size.

Comparison of the simulation results in Figure 2, with the minimum physical dislocation density plotted in Figure 1, suggests that a substantial range of these density plots lies below the physical limit of 1 net Burger's vector per Burger's circuit. This limit is not reflected in the plots of Figure 2 because the reported densities are averages over many Burger's circuits of the indicated size. Experimental data on real materials at these (sub-physical) densities would reflect variations in density from point to point, bounded from below by the resolution limit of the technique, and from above by the minimum physical dislocation density. Thus, in these simulations the plateau to the left of the graphs corresponds to the range of step sizes where every dislocation is resolved; however, it is only in the mean value of many Burger's circuits that the true (imposed) dislocation density is recovered.

It is a common misconception that a smaller step size will always lead to more accurate data. Instead, the opposite is often the case. As the step size decreases, the noise component of the data becomes increasingly dominant, and important information is lost. Instead, the selection of the method (Hough versus cross-correlation) and step size should be considered with an eye upon the expected dislocation density. As data is collected, alterations in method and step size may need to be considered, based upon preliminary results. Valid dislocation densities at a single material point occur only when those results lie above the resolution limits plotted in Figure 1. Statistical averaging over extended regions may resolve densities lying below the physical minimum density plotted in Figure 1, but errors in such averaging must consider the noise limitations of each method.

Next, as one proceeds to the right on the graphs in Figure 2, beyond the end of the upper plateau, the estimated dislocation density steadily decreases. This is due to dislocations of opposite signs cancelling each other within the Burgers' circuit. The slope of the descent closely parallels the slopes of the lines indicating the

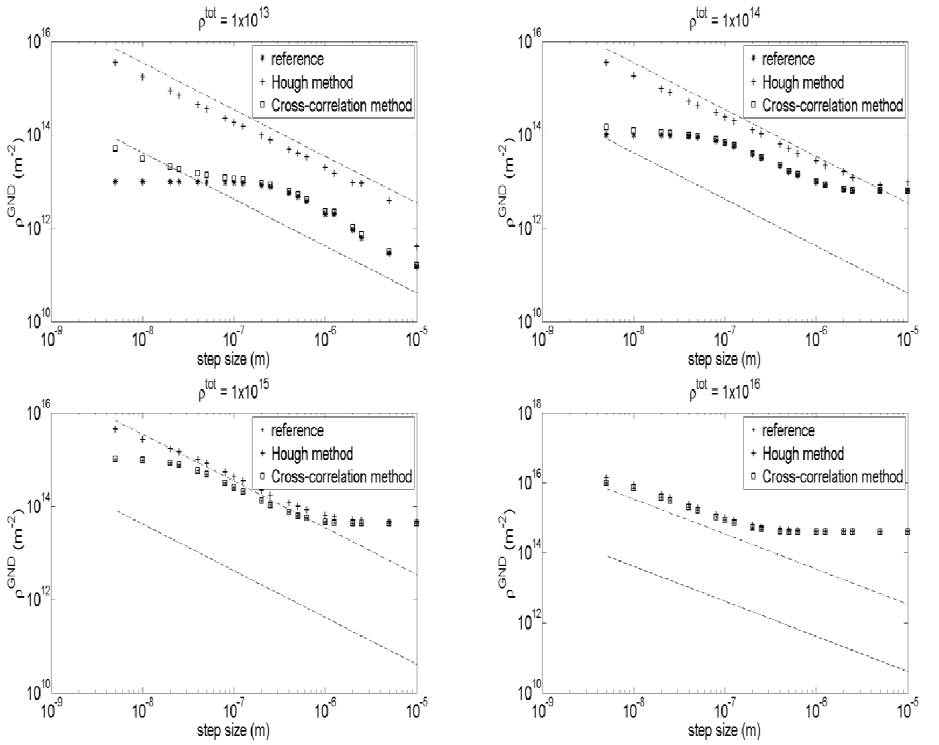

Figure 2: Simulations of dislocation density estimates. The standard deviation of the results between simulations was about 10^{12} m^{-2} for all simulations.

predicted resolution limit, which is as expected. However, the simulated dislocation density measurements consistently fall slightly below the predicted resolution limit (this can be seen most clearly in the upper left plot of Figure 1). This can be understood by taking into account that the plotted resolution limits are dictated by the maximum expected noise level. On average, the actual noise level will be slightly lower.

Proceeding further to the right on the plots of Figure 2, the data reach a second plateau at the larger step sizes. This plateau is related to the discrete nature of the simulations. Differences in the numbers of positive and negative Burger's vectors in the simulations give rise to an overall net Burger's vector for the complete region. The demarcation of this second plateau is the step size at which the maximum possible cancellation of multi-pole structures occurs. Within this second plateau the recovered dislocation density corresponds to the overall net Burger's vector of the simulated system. It is evident from the data presented in Figure 2 that the level

of polarization between positive and negative Burger's vectors is less than 10% for all simulations.

5 Experimental Evaluations

Experimental data were collected and analyzed as an evaluation of the simulations as well as a test to determine the effect of ignoring the elastic strain term when calculating the dislocation density tensor. The data were collected on a Philips XL30 S-FEG SEM operated at an accelerating voltage of 20 kV. EDAX/TSL's OIM software was used as the representative Hough-based method. The EBSD patterns were saved for offline cross-correlation analysis. A Matlab code was written by the authors for the offline cross-correlation analysis of the patterns.

Scans were collected from two different samples: a single crystal undeformed germanium sample and a 58% cold rolled copper sample. The copper sample was annealed for 1.5 hours at 225˚C after the cold rolling. The scans were taken upon a square grid at 20 nm step size over a 4x4 μm square region. Lattice orientation (Hough and cross-correlation) and elastic strain (cross correlation only) data were obtained at every point, and used to compute the dislocation density tensor. As a first order approximation, the total dislocation density was calculated as:

$$\rho_{Tot} = 9\langle|\alpha|\rangle \tag{7}$$

Here $\langle|\alpha|\rangle$ represents the average value of the absolute value of the available components of the dislocation density tensor. More sophisticated techniques for estimating the total dislocation density from the dislocation density tensor, accounting more completely for dislocation crystallography, can be found elsewhere [Sun, Adams et al 2000; Pantleon 2008).

In order to show the step size and angular resolution effects on the experimental data, the dislocation density was estimated using the information obtained by both OIM and the cross-correlation method. The step size was artificially increased by skipping an increasing number of scan points and the dislocation density was estimated at each step size. The dislocation density was then plotted as a function of step size for the data obtained using OIM, the cross-correlation method without the elastic strain term, and the cross-correlation method with the elastic strain term included (Figure 3).

When the density of dislocations associated with dipoles and multi-poles is low compared to the density of GNDs, their effect is more likely to become negligible at a smaller step size, leading to an earlier plateau (right side). This may explain the trends obtained from the deformed copper sample. There is no evidence of a right side plateau in the data taken from the germanium single crystal; and the mea-

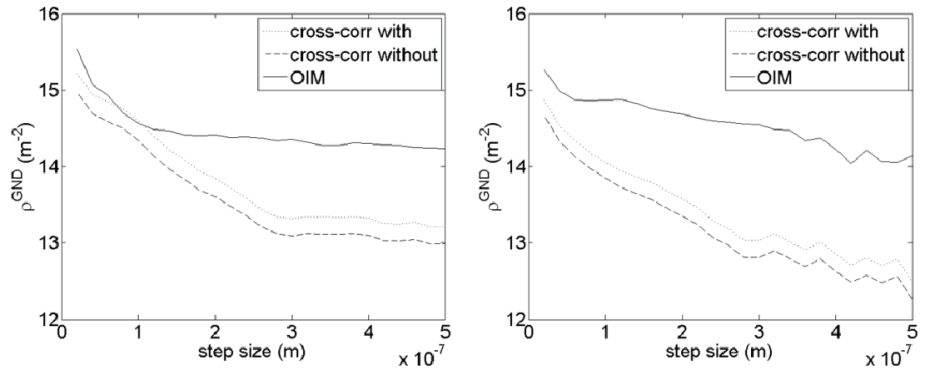

Figure 3: Total dislocation density measurement variations with step size from copper (left) and germanium single crystal (right). The y-axis is on a log scale.

sured trends correspond quite well to the low dislocation density simulation at the given range of step size. In neither case is there a plateau at small step size, suggesting that the total dislocation density (both statistically stored and geometrically necessary) is not reliably measured in the selected samples.

The experimental data also reconfirms that OIM in most cases is only able to measure higher than average local dislocation densities. This is especially apparent in the data taken from the germanium single crystal, where OIM estimates the dislocation density to be significantly higher than the density estimated using the cross-correlation method. In both cases, the OIM data has an upper plateau at $\sim 10^{14.5}$ m^{-2}. It would seem that OIM is incapable of making reliable estimates of the dislocation density below this level.

An interesting aspect displayed in the experimental data but excluded from the simulations is the effect of the elastic strain term on dislocation density estimations. In both samples, the inclusion of the elastic strain term caused the estimated dislocation density to increase. This increase is approximately independent of the step size, suggesting that the effects of the elastic strain gradients average in the same manner as orientation gradients.

6 Summary and Conclusions

It is quite evident, from the analysis and simulations presented in this paper, that the choice of step size for recovery of dislocation density field data by EBSD-based methods, is a complex one. Angular resolution is critical, and in all situations, the highest angular resolution method will give the most accurate results. Beyond this,

it is important to consider expected dislocation densities when selecting a suitable step size. With low dislocation density materials, such as the germanium single crystal presented in this study, small step sizes lead to erroneously high estimates of overall dislocation density – as can be seen by comparing Figures 3 and 1. Contrarily, for materials such as the deformed copper, where higher dislocation densities are expected, larger step sizes lead to significant averaging over multi-pole dislocation structures, resulting in a loss of potentially significant data.

Clearly, Hough-based techniques are capable of detecting only relatively large accumulations of dislocations. This makes Hough-based techniques useful for detecting dislocation pileups as might be expected to occur near grain boundaries or accumulations of dislocations that can occur at lower densities over larger length scales, but less effective when measuring low magnitude variations of dislocation density at small length scales. Based upon the work presented here, the resolution limit for ordinary Hough-based methods is $\sim 10^{14.5}\mathrm{m}^{-2}$. Cross-correlation methods offer almost two orders of magnitude improvement in angular resolution, making local low density dislocation structure characterization at high resolution much more feasible.

Although the simulated data presented in Figure 2 depict a (left) plateau that corresponds to step sizes that violate the physical minimum density shown in Figure 1, we have clarified that this is only possible when averaging over a statistically significant set of such measurements to obtain a mean value. Under experimental conditions where the goal is to evaluate the spatial fields of dislocation density, averaging is not appropriate, and individual measurement points must be evaluated in terms of their relationship to this physical minimum density and to the resolution limits of the method, which is governed by angular resolution.

Including the elastic strain gradient terms in estimates of the available components of the dislocation density tensor was found to increase the density estimates by a relatively uniform amount across the range of step sizes. This correction is of the order of $\sim$10-20% of the magnitude of density obtained when excluding these terms. In some situations it is anticipated that this correction could be significant.

It is evident that at this stage of EBSD development continued care is needed when interpreting EBSD-based dislocation estimates. Indeed, this paper presents evidence that some level of simulation may be required and useful to the interpretation of experimental results.

Acknowledgement: The authors wish to acknowledge funding for this work received from the Army Research Office, Dr. David Stepp Program Director.

References

Adams, B. L. (1997): Orientation imaging microscopy: Emerging and future applications. *Ultramicroscopy Proceedings of the 1996 6th onference on Frontiers in Electron Microscopy in Materials Science, Jun 4-7 1996* **67**(1-4): 11-17.

Kacher, J., . Landon, et al. (2009): Bragg's law diffraction simulations for electron backscatter diffraction analysis. *Ultramicroscopy* 10.1016/j.ultramic.2009.04.007.

Kroner, E. (1958): ontinuum theory of dislocations and self-stresses. *Ergebnisse der Angewandten Mathematik* **5**: 1327-1347.

Nye, J. F. (1953): Some geometrical relations in dislocated crystals. *Acta Metallurgica* **1**: 153-162.

Pantleon, W. (2008): Resolving the goemetrically necessary dislocation content by conventional electron backscattering diffraction. *Scripta Materialia* **58**: 994-997.

Schwartz, A. J., Kumar, M., and Adams, B.L. (2000): *Electron Backscatter Diffraction in Materials Science*. New York, Kluwer Academic/Plenum Publishers.

Sun, S., B. L. Adams, et al. (2000): Observations of lattice curvature near the interface of a deformed aluminium bicrystal. *Philosophical Magazine A: Physics of ondensed Matter, Structure, Defects and Mechanical Properties* **80**(1): 9-25.

Troost, K. Z., P. Van der Sluis, et al. (1993): Elastic strain determination by backscatter Kikuchi diffraction in the scanning electron microscope. *Applied Physics Letters* **62**(10): 1110-1112.

Wilkinson, A. J., G. Meaden, et al. (2005): Elastic Strain Tensor Mapping - extending the limits of EBSD analysis. *Microsc Microanal* **11**: 520-521.

Wilkinson, A. J., G. Meaden, et al. (2006): High-resolution elastic strain measurement from electron backscatter diffraction patterns: New levels of sensitivity. *Ultramicroscopy* **106**: 307-313.

Wright, S. I. (1993): Review of automated orientation imaging microscopy (OIM): *Journal of omputer-Assisted Microscopy* **5** (207).